Targeting APEX2 to the mRNA encoding fatty acid synthase β in yeast identifies interacting proteins that control its abundance in the cell cycle

Heidi M. Blank[a], Wendell P. Griffith[b], and Michael Polymenis[a,*]
[a]Department of Biochemistry and Biophysics, Texas A&M University, College Station, TX 77843; [b]Department of Chemistry, The University of Texas at San Antonio, San Antonio, TX 78249

ABSTRACT **Profiling the repertoire of proteins associated with a given mRNA during the cell cycle is unstudied. Furthermore, it is easier to ask and answer what mRNAs a specific protein might bind to than the other way around. Here, we implemented an RNA-centric proximity labeling technology at different points in the cell cycle in highly synchronous yeast cultures. To understand how the abundance of *FAS1*, encoding fatty acid synthase, peaks late in the cell cycle, we identified proteins that interact with the *FAS1* transcript in a cell cycle–dependent manner. We used dCas13d-APEX2 fusions to target *FAS1* and label nearby proteins, which were then identified by mass spectrometry. The glycolytic enzyme Tdh3p, a known RNA-binding protein, interacted with the *FAS1* mRNA, and it was necessary for the periodic abundance of Fas1p in the cell cycle. These results point to unexpected connections between major metabolic pathways. They also underscore the role of mRNA–protein interactions for gene expression during cell division.**

SIGNIFICANCE STATEMENT

- Proteins often interact with mRNAs, altering their fate and expression of the corresponding gene products.
- Cell cycle–dependent mRNA–protein interactions are poorly understood. Proximity labeling identified proteins interacting with a specific mRNA (FAS1) at different cell-cycle stages.
- An isoform of GAPDH (a protein involved in energy metabolism) interacted with FAS1 and was necessary to regulate the abundance of the Fas1p protein in the cell cycle.
- This demonstrates the utility of proximity labeling to study RNA–protein interactions in the context of the cell cycle and suggests the approach can be used to study RNA–protein interactions in other settings and temporal processes.

Monitoring Editor
Karsten Weis
ETH Zurich

Received: May 12, 2023
Revised: Sep 25, 2023
Accepted: Sep 29, 2023

New Methods

This article was published online ahead of print in MBoC in Press (http://www.molbiolcell.org/cgi/doi/10.1091/mbc.E23-05-0166) on October 4, 2023.

Conflict of interest: The authors have no conflicts of interest to declare that could be perceived to influence the presentation or interpretation of the data.

Author contributions: M.P. conceived and designed the study and wrote the first draft of the manuscript. W.P.G. performed the LC–MS/MS experiments. H.M.B. and M.P. performed all other experiments. All authors evaluated and discussed the data and edited the first draft.

*Address correspondence to: Michael Polymenis (michael.polymenis@ag.tamu.edu).

Abbreviations used: APEX2, ascorbate peroxidase 2; Cas13d, CRISPR associated protein 13d; DMSO, Dimethylsulfoxide; FDR, false discovery rate; gRNA, guide RNA; mRBP, mRNA binding protein; NADH, nicotinamide adenine dinucleotide –reduced; Ph, phenol.

INTRODUCTION

Proteins that bind to each mRNA could influence multiple steps in gene expression, impacting the mRNA's processing, stability, or interaction with ribosomes and translation. The repertoire of protein–mRNA interactions has been traditionally defined from protein-centric methods, tagging a given mRNA-binding protein (mRBP), and answering what mRNAs bind to the mRBP (Hogan *et al.*, 2008). The converse, mRNA-centric approach to identify what proteins a specific mRNA binds is challenging because it requires tagging the mRNA of interest. Recently, new technologies, including engineered CRISPR-Cas systems, have been implemented to target particular mRNAs (Abudayyeh *et al.*, 2017; Han *et al.*, 2020; Li *et al.*, 2021). When combined with ascorbate peroxidase (APEX)-based or similar proximity-labeling tools, proteins interacting with the RNA of interest can be identified (Han *et al.*, 2020; Li *et al.*, 2021).

There are several unexplored contexts where identifying mRNA–mRBP interactions could offer significant biological insight. For example, in recent years, ribosome profiling experiments have identified mRNAs that are translated with different efficiency during cell division in bacterial (Schrader *et al.*, 2016), human (Stumpf *et al.*, 2013; Tanenbaum *et al.*, 2015) or yeast cells (Maitra *et al.*, 2020; Blank *et al.*, 2017b). A key question is how translational control can be imposed when protein synthesis rates remain unchanged as cells progress in the cell cycle (Elliott and McLaughlin, 1978; Tanenbaum *et al.*, 2015; Stonyte *et al.*, 2018). Changes in ribosome abundance resulting, for example, from nutrient changes, impose straightforward translational control on specific mRNAs (Mills and Green, 2017). But the ribosome content does not change in the cell cycle (Elliott *et al.*, 1979; Blank *et al.*, 2020). On the other hand, specific mRBP–mRNA interactions could establish translational control during cell division.

Several mRBPs have altered levels in the cell cycle, their loss-of-function mutations lead to cell-cycle phenotypes, or they are targeted by the cyclin-dependent kinase (Cdk) that drives cell-cycle transitions (Polymenis, 2022a). However, there are few examples of mRBP–mRNA interactions with known roles during cell division. The best case in budding yeast is Whi3p, which binds the G1 cyclin *CLN3* mRNA. The Whi3p–*CLN3* interactions destabilize *CLN3* and also repress its translation (Cai and Futcher, 2013). In mammals, the DENR-MCT1 heterodimer is phosphorylated by mitotic Cdk/cyclin complexes, enabling it to derepress the translation of specific mRNAs needed for the proper execution of mitosis (Clemm von Hohenberg *et al.*, 2022). These examples notwithstanding, there is little additional information on mRBP–mRNA interactions significant for cell division. To fill this gap in knowledge, it is necessary to examine dynamic mRBP–mRNA interactions in highly synchronous cells as they progress in the cell cycle.

Past work probing RNA–protein interactions revealed several metabolic enzymes moonlighting as RNA-binding proteins (Beckmann *et al.*, 2015; Hentze *et al.*, 2018). For example, the glycolytic enzyme GAPDH, which converts glyceraldehyde-3-phosphate and NAD^+ to 1,3-bisphosphoglycerate and nicotinamide adenine dinucleotide–reduced (NADH), binds to multiple RNAs in mammalian (Ryazanov, 1985; Singh and Green, 1993; Dollenmaier and Weitz, 2003; Bonafé *et al.*, 2005; Rodríguez-Pascual *et al.*, 2008; Castello *et al.*, 2016) and yeast (Hogan *et al.*, 2008; Mitchell *et al.*, 2013; Matia-González *et al.*, 2015) cells. These enzyme–RNA interactions may influence not only the target RNA but also the enzyme's catalytic activity (e.g., by blocking access to its metabolite substrates), leading to the formulation of the RNA-enzyme-metabolite (REM) hypothesis of metabolic and gene expression control (Hentze and Preiss, 2010). Nonetheless, in most cases, the physiological function of the RNA-binding activity of metabolic enzymes and whether they regulate their target mRNAs remain unknown (Castello *et al.*, 2015).

Here, we describe the application of RNA-centric proximity labeling in yeast and the first cell cycle–dependent interrogation of mRBP–mRNA interactions in any system. We had previously reported the identification of mRNAs with altered translational efficiency in the cell cycle (Blank *et al.*, 2017b). Among these mRNAs was *FAS1*, encoding the β subunit of fatty acid synthase. The translational efficiency of *FAS1* and the levels of the fatty acid synthesis (Fas1p) protein peak late in the cell cycle, providing lipid resources needed for mitosis (Blank *et al.*, 2017a, 2017b; Maitra *et al.*, 2022). We implemented dCas13d-APEX2–mediated proximity labeling to identify proteins interacting with the *FAS1* mRNA in a cell cycle–dependent manner. Our results suggest that Tdh3p, a yeast GAPDH isoform, interacts with *FAS1* and it is necessary to promote Fas1p synthesis late in the cell cycle. These results reveal unexpected gene expression control layers during cell division. Furthermore, they point to possible connections between enzymes of major metabolic pathways, such as lipogenesis (Fas1p) and glycolysis (Tdh3p). Lastly, the approaches we used can apply to other systems.

RESULTS AND DISCUSSION

Generating active dCas13d-APEX2 targeting the *FAS1* mRNA in yeast

To bring APEX2 to the *FAS1* transcript, we decided to deploy in yeast the CRISPR-Cas13d targeting approach reported recently for mammalian cells (Han *et al.*, 2020). Although dCas13d (encoding a catalytically dead, guide RNA [gRNA]-directed ribonuclease) targets exclusively RNA (Zhang *et al.*, 2018), for proximity labeling applications, the interaction is stabilized by adding a double-stranded RNA-binding domain (dsRBD; Han *et al.*, 2020). To drive the expression of dCas13d–dsRBD–APEX2 in yeast, we placed this construct (C-terminally tagged with the V5 epitope for protein surveillance purposes) under the control of a strong promoter (Figure 1A). In the same integrative plasmid, we also placed in a bicistronic arrangement the necessary sequences for the expression of a gRNA (Figure 1A; see *Materials and Methods*). We chose three predicted gRNA sequences for Cas13 systems (Wessels *et al.*, 2020), targeting the long *FAS1* transcript (~6.5–7 kb) at the positions shown in Figure 1B (see also *Materials and Methods*). Each of the three bicistronic constructs, carrying both the dCas13d–dsRBD–APEX2-V5 and one of the gRNA cistrons, was then integrated at the *URA3* locus, generating three yeast strains (*FAS1-1*, *FAS1-2*, and *FAS1-3*) that were used in our subsequent proximity labeling experiments.

To test whether APEX activity is present in the yeast cells, we exposed them to hydrogen peroxide and Amplex Red, which in an APEX2-catalyzed reaction is oxidized to the fluorescent product resorufin (Dębski *et al.*, 2016). Cells from all three strains expressing dCas13d–dsRBD–APEX2-V5 along with a *FAS1* gRNA became highly fluorescent compared with the parental strain that does not express APEX2 (Figure 1C). Furthermore, using the V5 epitope, we immunoprecipitated dCas13d–dsRBD–APEX2-V5 and asked whether the *FAS1* mRNA was associated with it, as measured by digital droplet PCR (ddPCR; see *Materials and Methods*). We found a moderate (~1.5–2-fold) but significant ($p < 0.0001$, based on the robust bootstrap ANOVA; see *Materials and Methods*) enrichment of *FAS1* levels in the immunoprecipitated samples compared with the input levels in the cell extracts (Figure 1D). There was no significant enrichment for *FAS1* in precipitates from cells carrying the APEX construct and no targeting gRNA (NT-APEX), or cells without the APEX construct

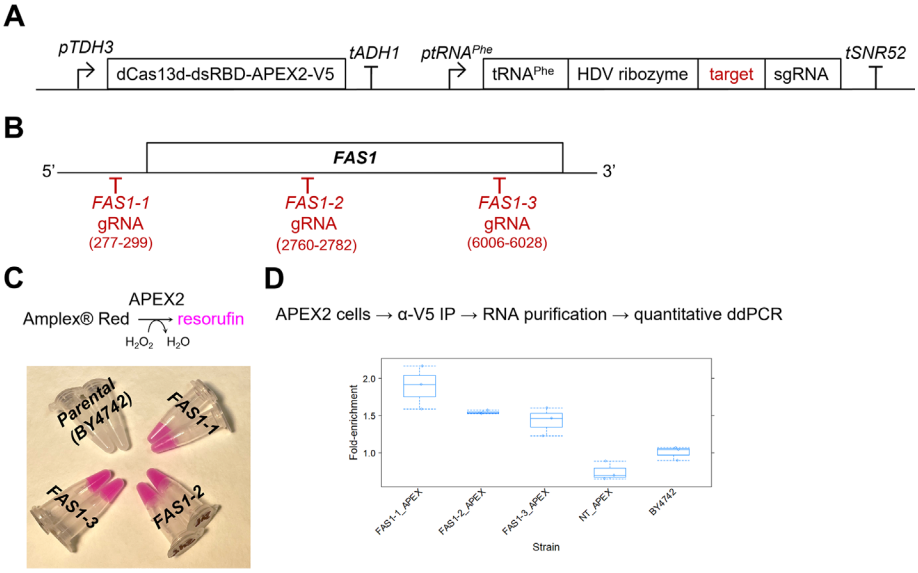

FIGURE 1: Engineered yeast cells express active dCas13d-APEX2 targeting the *FAS1* mRNA. (A) Diagram of the engineered bicistronic locus introduced into yeast cells to express dCas13d-APEX2 and gRNAs targeting *FAS1* (see *Materials and Methods*). (B) Schematic of the targeted positions on the *FAS1* mRNA. (C) Cells of the indicated genotype, carrying different gRNAs targeting *FAS1*, express active APEX2 based on the conversion of Amplex Red to resorufin. The cells were processed as described in *Materials and Methods*. (D) Yeast cells expressing dCas13d-dsRBD-APEX2-V5, see A, target it preferentially to the *FAS1* mRNA (ddPCR; see *Materials and Methods*) was used to measure the levels of *FAS1* immunoprecipitated by dCas13d-dsRBD-APEX2-V5. The fold enrichment is on the y-axis, from the strains shown on the x-axis carrying the APEX construct and each of the *FAS1* gRNAs depicted in (B), a strain expressing nontargeted APEX (NT_APEX; carrying the APEX-TU1 construct, see *Materials and Methods*), or the parental strain (BY4742). Transcript levels of *FAS1* were normalized against the corresponding transcript levels of *UBC6* (see *Materials and Methods*). The values used to generate the graphs are in Supplemental File S1/Sheet 1.

(BY4742; Figure 1D). We note that in the published example of dCas13d–dsRBD–APEX2-V5 targeted to the human telomerase RNA, the reported enrichment was three- to fourfold (Han *et al.*, 2020). These results suggest that dCas13d–dsRBD–APEX2-V5 was active in yeast cells and targeted the *FAS1* transcript.

Establishing labeling conditions in cells expressing dCas13d–APEX2 fusions

Our next objective was to establish the conditions necessary to observe labeling, reported by the appearance of biotinylated proteins. APEX labeling has not been very successful in yeast because yeast cells are impermeable to biotin-conjugated phenol, which needs to be oxidized by the APEX peroxidase into its reactive, free-radical form before it can form covalent bonds with electron-rich groups, such as those found on the side chains of amino acids. It has been reported that weakening the cell wall with zymolyase (Hwang and Espenshade, 2016) or osmotic shock with freeze–thaw cycles (Singer-Krüger *et al.*, 2020) improves APEX-mediated labeling. An alternative strategy relies on the cellular uptake of a chemical probe that affixes to targets via APEX labeling. The chemical group is then derivatized with click chemistry in vitro, in cell extracts, to attach biotin to the labeled targets (Li *et al.*, 2020). We tried all the above procedures, but with limited success. Osmotic shock with freeze–thaw cycles did improve the observed labeling, based on the appearance of biotinylated proteins on immunoblots (Figure 2; compare the first lane revealing the endogenous biotinylated yeast proteins to the second lane revealing the increased APEX-mediated labeling by osmotic shock). To achieve more efficient labeling, in addition to osmotic shock, we relied on a previously described approach, employing digitonin permeabilization, to measure glycolysis in situ (Cordeiro and Freire, 1995). As we detail in *Materials and Methods*, permeabilization of cells with digitonin (used at 0.01%) resulted in strong labeling and appearance of biotinylated proteins (Figure 2; see last five lanes). These results argue that we had in place the necessary tools and experimental conditions to identify the proteins interacting with the *FAS1* transcript.

Proximity labeling of proteins targeting *FAS1* in the cell cycle

We relied on centrifugal elutriation to collect synchronous cells because it is a selection method that is less disruptive of the normal coordination between cell growth and division than arrest-and-release methods (Aramayo and Polymenis, 2017; Polymenis, 2022b). To overcome the low yield associated with elutriation, we generated pools of cells collected at the same cell size, as we have done in the past (Blank *et al.*, 2017b; Maitra *et al.*, 2020). Because yeast daughter cells actively monitor their size to adjust progression in the cell cycle (aka "sizer" behavior; Di Talia *et al.*, 2007), their position in the cell cycle is reflected by how big they are. From a total of 54 elutriated cultures (Figure 3A), for each of the three engineered strains (FAS1-1, FAS1-2, and FAS1-3), we generated three pools of small, unbudded G1 cells and three pools of large, budded, non-G1 cells (Figure 3B). Each pool consisted of ~1E+09 cells, and it was processed for APEX proximity labeling as described in *Materials and Methods*.

Biotinylated proteins were precipitated with streptavidin magnetic beads, digested with trypsin, and subjected to mass spectrometry for protein identification (see *Materials and Methods*). We identified 937 unique peptides in the precipitated samples (Supplemental File S1/Sheet 3). These peptides were assigned to 456 proteins (Supplemental File S1/Sheet 4). The list also included naturally biotinylated yeast proteins, such as Acc1p (Al-Feel *et al.*, 1992; Schneiter *et al.*, 1999). The output of the gene ontology enrichment based on molecular function of the proteins we identified is shown in Supplemental File S1/Sheet5. By far, the most enriched groups were related to RNA binding ($n = 127$), translation factor activity:RNA binding ($n = 24$), and structural ribosome constituents ($n = 91$). The highest enrichment (~10-fold) was for "sequence-specific mRNA binding"; GO:1990825' ($p = 1.38E-09$, false discovery rate (FDR) = 1.4E-07).

As a proxy for the relative abundance of the proteins we identified, we used their exponentially modified protein abundance index scores (Ishihama *et al.*, 2005). For each of the three strains, we then used robust bootstrap ANOVA to identify proteins whose abundance changed significantly in G1 versus non-G1 cells ($p < 0.05$ and fold-change ≥ 2; see Figure 3C; Supplemental File S1/Sheet 3). The levels of 52 proteins changed significantly in the immunoprecipitated samples in G1 versus non-G1 cells (Figure 3D, right set).

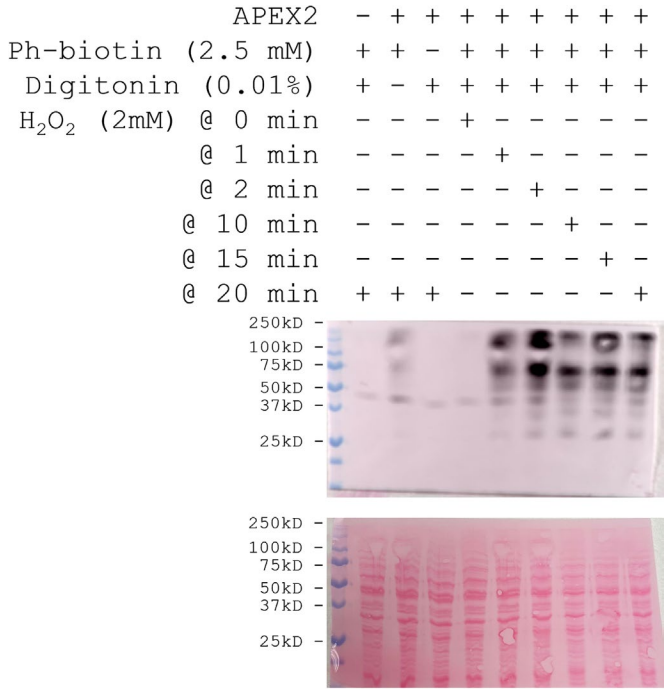

FIGURE 2: Biotin labeling conditions in cells expressing dCas13d-APEX2 fusions. The immunoblot displays the signal from biotinylated proteins in cells treated in each condition shown on top. The first lane is from extracts prepared using strain BY4742, and the rest is from extracts using strain *FAS1-1*. The blot at the bottom is the one shown above before it was processed for immunodetection, stained with Ponceau S to reveal total protein loading.

Another 51 proteins were found exclusively in G1 or non-G1 cells, but not both (Figure 3D, left set), raising the total to 103 putative hits (Supplemental File S1/Sheet 6). We note that the interactions we identified with the *FAS1* mRNA are proximity-based and may not necessarily be direct.

Among the 103 proteins we identified, 67 were previously included in a list of 765 yeast proteins that bound RNAs in vivo ([Matia-González *et al.*, 2015]; shown as the "PMID_2695419_ mRBPs" set in Figure 3D), potentially attesting to the power of our approach. However, that reference compendium was rather expansive, including, for example, ribosomal proteins and known DNA helicases (Matia-González *et al.*, 2015). Furthermore, because *FAS1* is abundant, one could envision spurious interactions among these 103 proteins. Hence, to prioritize our hits for follow-up studies, we also looked at a smaller reference set of 306 yeast mRBPs (Polymenis, 2022a) based on earlier in vivo RNA interactome studies ([Hogan *et al.*, 2008; Mitchell *et al.*, 2013]; shown as the "PMID_35618506_ mRBPs" set in Figure 3D). Only five of the 103 proteins we identified here to interact in a cell cycle–dependent manner with *FAS1* were in both reference mRBP sets (Figure 3D). These five proteins were: Arc1p, Dps1p, Sro9p, Ssd1p, and Tdh3p.

Arc1p is involved in tRNA delivery and binds tRNAs and methionyl- and glutamyl-tRNA synthetases (Simos *et al.*, 1996), while Dps1p is an aspartyl-tRNA synthetase (Sellami *et al.*, 1985). Sro9p has a La-motif involved in RNA binding and it is associated with ribosomes (Sobel and Wolin, 1999). Ssd1p binds and represses mRNAs, especially ones involved in cell wall biosynthesis (Kaeberlein and Guarente, 2002; Bayne *et al.*, 2022). Tdh3p is one of three GAPDH isoforms in yeast (McAlister and Holland, 1985). Regarding their binding to the *FAS1* mRNA, the cell cycle–specific enrichment of all five proteins was highly significant ($p < 0.0001$, based on the robust bootstrap ANOVA). Interestingly, except for Sro9p, identified from strain FAS1-1 expressing a gRNA from the 5′-UTR of the *FAS1* transcript, all others were identified from strain FAS1-2, which expresses a gRNA from the middle of the *FAS1* transcript (Figure 1B). Lastly, while Tdh3p interacted with the *FAS1* mRNA preferentially late in the cell cycle, all other proteins did so in the G1 phase (Figure 3E).

We next tested whether the abundance of any of these proteins changed in the cell cycle. We used strains carrying TAP-tagged alleles of the corresponding gene. Except for *DPS1-TAP*, all other strains were commercially available (see *Reagent Table*), expressing TAP-tagged proteins (Arc1p, Sro9p, Ssd1p, and Tdh3p) of the expected size (Supplemental Figure S1; Supplemental File S2). Attempts to generate a *DPS1-TAP* strain were unsuccessful, so we proceeded with the rest. We isolated early G1 cells by centrifugal elutriation. We measured their size and budding as cells progressed in the cell cycle and collected samples for immunoblotting at regular intervals. The abundance of all four proteins was not periodic (Supplemental Figure S1). We note that the levels of the corresponding mRNAs encoding these proteins also do not change in the cell cycle (Spellman *et al.*, 1998; Santos *et al.*, 2015; Blank *et al.*, 2017b, 2020). Hence, the cell cycle–dependent interaction of these proteins detected in our proximity labeling experiments does not arise from changes in their levels in the cell cycle.

Tdh3p interacts with *FAS1*, and it is required for cell cycle–dependent changes in Fas1p levels

To follow up on the findings from our proximity labeling experiments, we performed the reciprocal, protein-centric experiments to test the mRBP interactions with the *FAS1* transcript. We pulled down the TAP-tagged proteins from asynchronous cultures, and asked whether *FAS1* levels were enriched in the precipitates (see *Materials and Methods*). We found that *FAS1* levels were not enriched with the precipitated Arc1p-TAP, Sro9p-TAP, or Ssd1p-TAP proteins, but *FAS1* was significantly associated with Tdh3p-TAP (Figure 4A; $p < 0.0001$, based on the robust bootstrap ANOVA). These results do not necessarily exclude the possibility that Arc1p, Sro9p, or Ssd1p interact with *FAS1* in cells. These interactions may be transient and missed in pull-down experiments but detected by APEX-mediated proximity labeling. We also note that previously reported RNA interactomes typically involve a UV crosslinking step (Mitchell *et al.*, 2013; Matia-González *et al.*, 2015; Hentze *et al.*, 2018), to capture weak RNA–protein interaction. We did not use UV crosslinking in our experiments. Nonetheless, because the Tdh3p interactions with *FAS1* were evident in both approaches we used (RNA proximity labeling and protein pull downs), we focused on Tdh3p's role in mediating the cell cycle–dependent changes in the abundance of Fas1p.

For Fas1p surveillance in the cell cycle, we used cells carrying a *FAS1-TAP* allele expressed from its native chromosomal locus and introduced a *TDH3* or *ARC1* deletion (the latter used as an additional control in this experiment because we saw no binding of Arc1p to *FAS1* in the immunoprecipitations; see Figure 4A). From synchronous elutriated cultures, we found that while Fas1p levels increased markedly late in the cell cycle in wild-type and *arc1*Δ cells, they remained constant in *tdh3*Δ cells (Figure 4B). We conclude that Tdh3p is necessary for the cell cycle–dependent changes in Fas1p levels, arguing for a physiological role for the Tdh3p–*FAS1* interactions.

The above experiments allowed us also to evaluate cell-cycle kinetics in cells lacking Tdh3p or Arc1p. As we mentioned above, daughter budding yeast cells actively monitor their size before passing a commitment step in late G1, called Start, and initiate DNA replication. For any given strain and nutrient environment, a highly

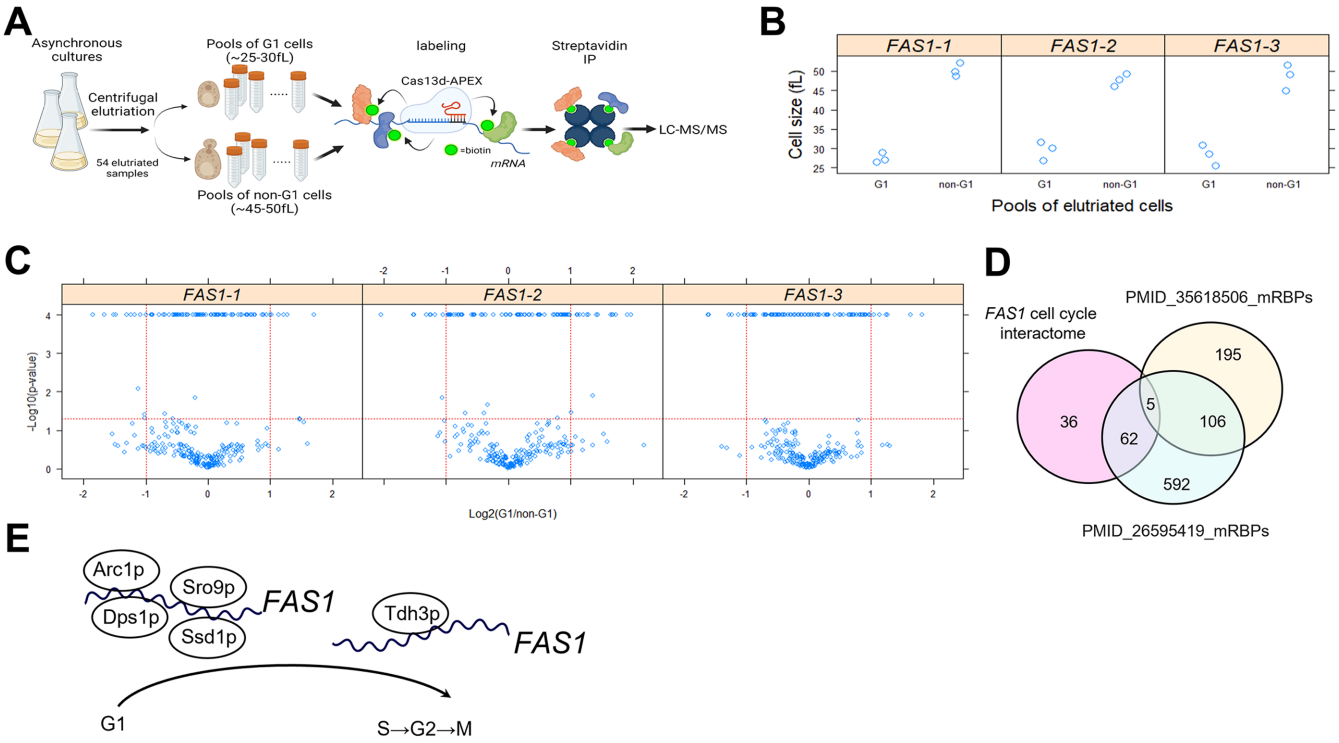

FIGURE 3: Proximity labeling of proteins targeting *FAS1* in the cell cycle. (A) Schematic overview of our experimental approach. This panel was created with BioRender.com. (B) The cell size (y-axis) of the pools of cells we isolated from each strain is shown for the G1 and non-G1 cells (x-axis). The values used to generate the graphs are in Supplemental File S1/Sheet2. C) Volcano plots depicting the proteins identified by mass spectrometry in the indicated strain (shown above each panel) whose levels changed significantly in G1 versus non-G1 cells, based on the magnitude of the difference (x-axis; Log2-fold change) and statistical significance (y-axis), indicated by the red lines. The analytical and statistical approaches are described in *Materials and Methods*. The values used to generate the graphs are in Supplemental File S1/Sheet3. Note that the lowest calculated *p* values from the robust ANOVA were at the 0.0001 level. The input values used in the ANOVA analyses are in Supplemental File S1/Sheets 6, 7, and 8. D) Venn diagram of the proteins we identified to interact with *FAS1* in a cell cycle–dependent manner (left set) against two reference sets (PMID_35618506, right; and PMID_26595419, middle). The values used to generate the graph are in Supplemental File S1/Sheet 9. (E) Schematic summary of the mRBPs that bind the *FAS1* transcript in G1 or non-G1 phases.

reproducible parameter reflecting the timing of Start is the "critical size" (Polymenis, 2022b), defined functionally here as the size at which 50% of the cells are budded. We found that cells lacking either Tdh3p or Arc1p have a larger critical size than otherwise wild-type cells (Figure 5A), consistent with delayed Start. However, the rate at which these cells increased in size was similar to that of wild-type cells (Figure 5B). From asynchronous cultures of these strains, we noticed that cells lacking Tdh3p or Arc1p were bigger (Figure 5C, left panel), and *tdh3*Δ cells also appeared to have a larger birth size than their wild-type counterparts (Figure 5C, right panel).

We stress that these cell-cycle phenotypes are not necessarily related to the interactions of these mRBPs with *FAS1* or other mRNAs. For example, it is more likely that the major role of Tdh3p in central metabolism underpins the cell-cycle phenotypes of *tdh3*Δ mutants. Interestingly, however, our results argue for rather specific effects of these mRBPs on size homeostasis (Figure 5C) and cell-cycle progression (Figure 5A), which do not arise from severe growth defects (Figure 5B). In particular, loss of Tdh3p delays the G1/S transition, reflected in the larger critical size of *tdh3*Δ cells, and also delays exit from mitosis, accounting for the larger birth size of *tdh3*Δ cells (Figure 5C, right panel). Hence, the phenotypic consequences on cell-cycle progression upon Tdh3p loss are distinct from generic growth impairments, typically leading to smaller mean and birth cell sizes (Polymenis, 2022b).

Concluding remarks

Our results highlight the role of a key glycolytic enzyme (Tdh3p) through its moonlighting RNA-binding properties in the expression of another enzyme (Fas1p) involved in fatty acid biosynthesis. The Tdh3p:*FAS1* interaction is physiologically relevant because it imparts temporal control of Fas1p synthesis, peaking late in the cell cycle. Such interactions could contribute to the temporal compartmentalization of major metabolic pathways during cell division, which based on recent single-cell microscopy studies may be a general feature (Takhaveev *et al.*, 2023). Although *FAS1* is translationally controlled in the cell cycle, its interaction with Tdh3p may not necessarily affect its translational efficiency. Interactions between mRNAs and mRBPs could change gene expression in many ways, including changing the localization or stability of mRNAs. Why the Tdh3p:*FAS1* interaction is prominent late in the cell cycle is not clear. We showed that Tdh3p levels do not change in the cell cycle (Supplemental Figure S1). On the other hand, Tdh3p is heavily modified by glycosylation (Zielinska *et al.*, 2012; Cao *et al.*, 2014), ubiquitination (Swaney *et al.*, 2013; Back *et al.*, 2019), succinylation (Weinert *et al.*, 2013; Frankovsky *et al.*, 2021), acetylation (Henriksen *et al.*, 2012), sumoylation (Bhagwat *et al.*, 2021), methylation (Wang *et al.*, 2015), and phosphorylation (Albuquerque *et al.*, 2008; Holt *et al.*, 2009; Soulard *et al.*, 2010; Rødkær *et al.*, 2014; MacGilvray *et al.*, 2020; Lanz *et al.*, 2021; Zhou *et al.*, 2021). Changes in these posttranslational modifications

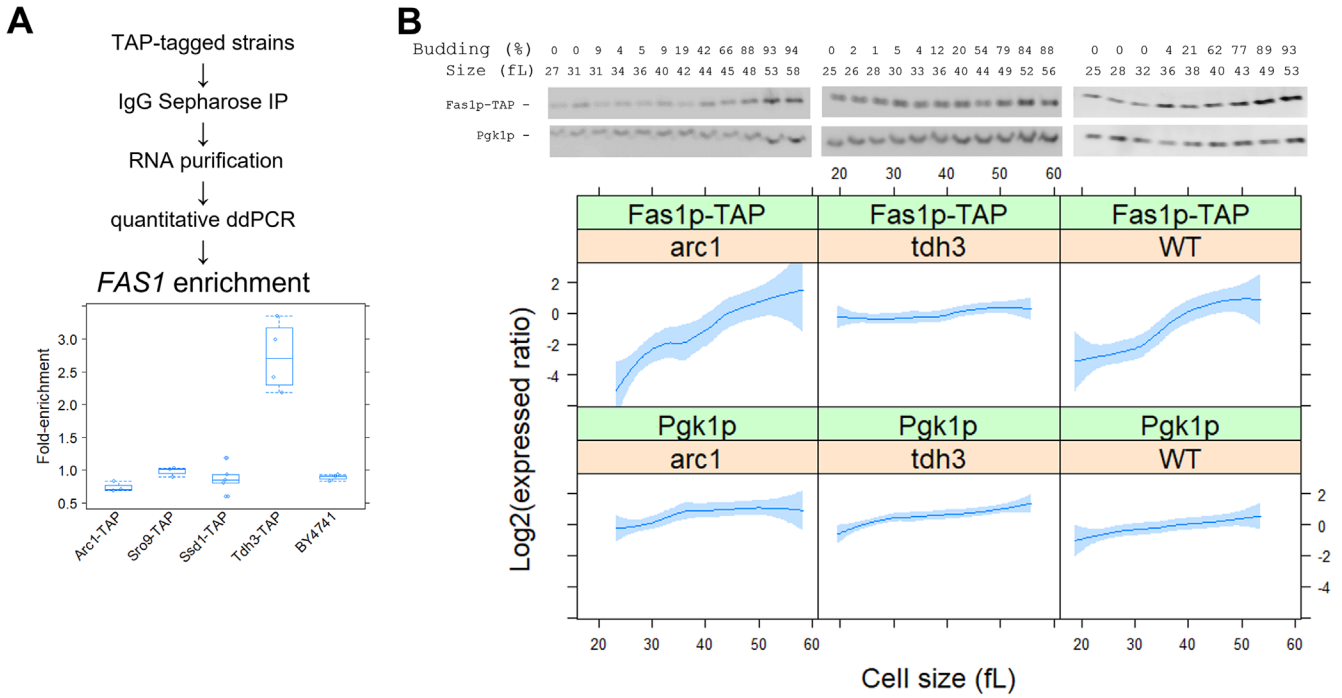

FIGURE 4: Tdh3p binds *FAS1*, and it is required for cell cycle–dependent changes in Fas1p levels. (A) Yeast cells expressing the corresponding TAP-tagged alleles were used to immunoprecipitate the indicated TAP-tagged proteins. The levels of the associated *FAS1* mRNA in the immunoprecipitates (measured as in Figure 1D; see *Materials and Methods*) are shown on the y-axis in the strains shown on the x-axis. Transcript levels of *FAS1* were normalized against the corresponding transcript levels of *UBC6*. The values used to generate the graphs are in Supplemental File S1/Sheet 10. B) The abundance of TAP-tagged proteins was monitored in strains of the indicated genotype, as described in *Materials and Methods*. Samples were collected by elutriation in a rich, undefined medium (YPD) and allowed to progress synchronously in the cell cycle. Experiment-matched loading controls (measuring Pgk1p abundance) were also quantified and shown in parallel. (Top), representative immunoblots, along with the percentage of budded cells (percentage budded) and the cell size (in fL) for each sample. (Bottom), from at least three independent experiments in each case, the TAP and Pgk1p signal intensities were quantified as described in *Materials and Methods*. The Log2 (expressed ratios) values are on the y-axis, and cell size values are on the x-axis. Loess curves and the standard errors at a 0.95 level are shown. All the immunoblots for this figure are in Supplemental File S2, while the values used to generate the graphs are in Supplemental File S1/Sheet 11.

could modulate the RNA-binding properties of Tdh3p. For example, we note that Tdh3p is targeted by the Cdk at 14 sites (Holt *et al.*, 2009). More generally, our results describe the tools and methods to identify cell cycle–dependent interactions between a particular mRNA and proteins in yeast and other systems.

MATERIALS AND METHODS

Request a protocol through *Bio-protocol*.

A Reagent Table (Supplemental File S4) is in the Supplementary Files. Where known, the Research Resource Identifiers (RRIDs) are shown in the Reagent Table.

Media and growth conditions

For bacterial growth during cloning procedures, we used NEB 5-alpha Competent *Escherichia coli* (high efficiency) cells from New England Biolabs (catalogue #: C2987H), grown in standard LB medium (1% $^{wt/vol}$ tryptone, 1% $^{wt/vol}$ NaCl, 0.5% $^{wt/vol}$ yeast extract, pH 7.0) at 37°C with the appropriate antibiotic to maintain plasmid selection. All the *Saccharomyces cerevisiae* strains used in this study are shown in the Reagent Table. For most experiments, the cells were cultivated in the standard, rich, undefined medium YPD (1% $^{wt/vol}$ yeast extract, 2% $^{wt/vol}$ peptone, 2% $^{wt/vol}$ dextrose), at 30°C (Kaiser *et al.*, 1994).

Plasmids and strains

dCas13d-dsRBD-APEX2 entry plasmid. The dCas13d-dsRBD-APEX2 plasmid, originally engineered for mammalian expression, was a gift from Alice Ting (Addgene plasmid catalogue # 154939; http://n2t.net/addgene:154939; RRID:Addgene_154939), generated as described in (Han *et al.*, 2020). With that plasmid as a template, sequences corresponding to positions 1-603, and 604-4071, of the insert were amplified with Phusion High-Fidelity DNA Polymerase, using primers APEX_1-603_fwd and APEX_1-603_rev and APEX_604-4071_fwd and APEX_604-4071_rev, respectively. The primers were designed to enable *Bsm*BI/*Bsa*I assembly of the full-length (positions 1-4071) dCas13d-dsRBD-APEX2 insert into the entry vector (plasmid YTK001) of the MoClo-YTK plasmid kit (Lee *et al.*, 2015), which was a gift from John Dueber (Addgene kit # 1000000061). Note that the insert sequences were amplified in two separate fragments, to remove an internal type IIS restriction site that would interfere with downstream "Golden Gate" cloning strategies. The YTK001 vector and the amplified fragments were subjected to single-pot "Golden Gate" assembly (Engler *et al.*, 2008, 2009).

The assembly reaction contained 1 µl of each DNA fragment (from a 20 fmol/µl solution), 1.5 µl T4 ligase buffer (from a 10× solution), 1 µl of T7 ligase, 0.5 µl of restriction enzyme (*Bsm*BI in this case), and water to 15 µl total reaction volume. Unless

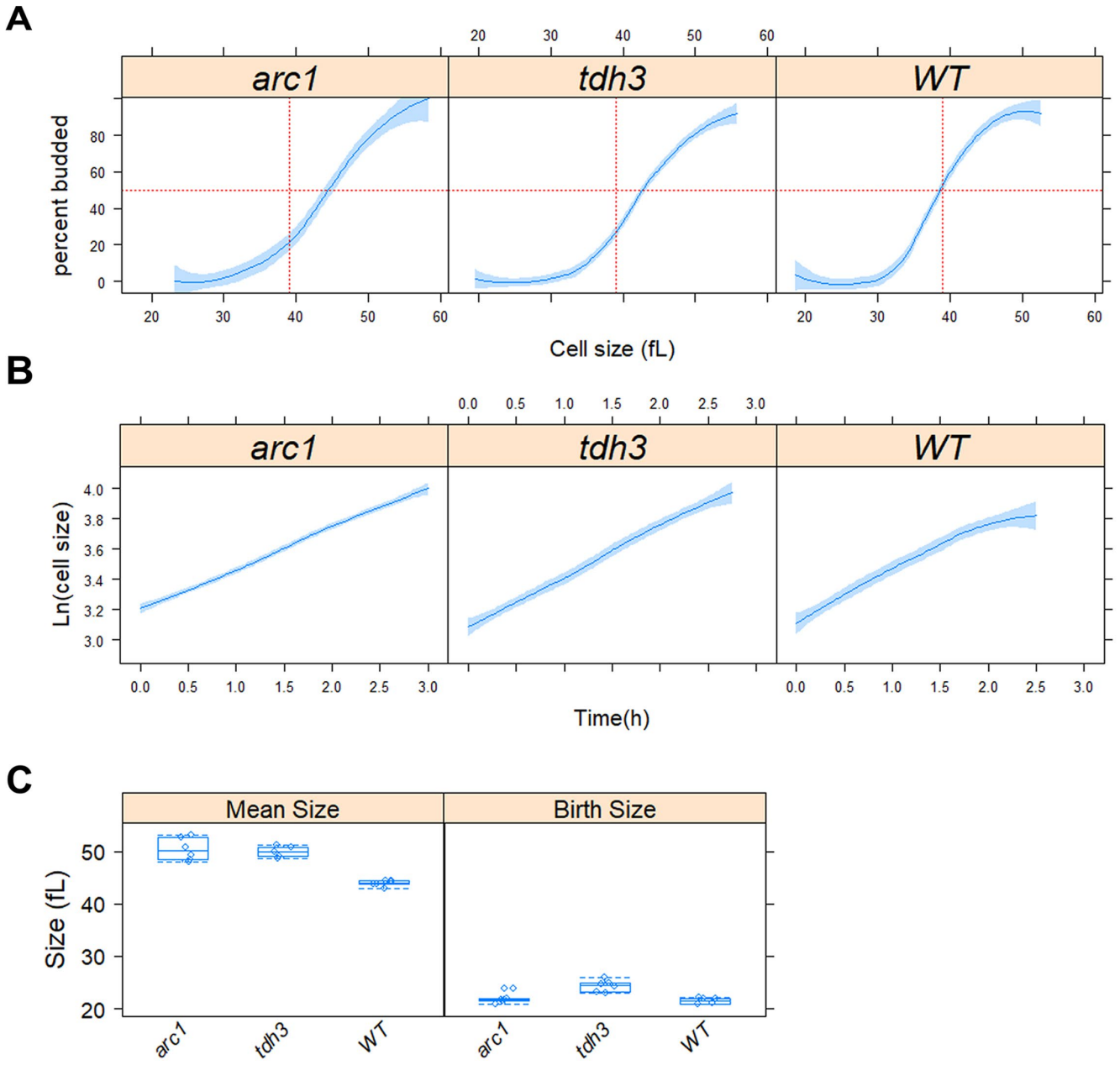

FIGURE 5: Altered cells size homeostasis and cell-cycle kinetics in cells lacking Tdh3p. (A) From the synchronous cultures shown in Figure 4B, the percentage of budded cells (y-axis) is shown against the mean cell size (in fL; x-axis). Loess curves and the standard errors at a 0.95 level are shown. (B) From the same experiments as above, the rate of size increase is indicated from the plots of the Ln-transformed cell size values (y-axis) against time (x-axis). The values used to generate the graphs in A and B are in Supplemental File S1/Sheet 11. (C) Box plots showing the mean (left panel) and birth (right panel) size (y-axis) for the indicated strains. Comparisons were made with the nonparametric Kruskal-Wallis rank sum test, and the indicated *p* values calculated from the pairwise comparisons using the Wilcoxon rank sum test with continuity correction, using R language functions. The values used to generate the graphs are in Supplemental File S1/Sheet 12.

indicated otherwise, the same reaction composition was used for all assemblies.

The reaction conditions were 30 cycles: 42°C for 1 min, 16°C for 1 min; followed by 60°C for 5 min. The correct assembly of the resulting plasmid (APEX_ENTRY) was verified by sequencing of the entire 4071 bp insert, with primers FOR_1, FOR_2, FOR_3, FOR_4, FOR_5, FOR_6, and REV_1 (see *Reagent Table*).

***FAS1* gRNA entry plasmids.** To design Cas13 RNAs (cRNAs), we used the web-based platform developed by Sanjana and colleagues (Wessels *et al.*, 2020). The three RNAs we chose corresponded to positions near the start (positions 277-299), middle (positions 2760-2782), and end (positions 6006-6028) of the *FAS1* mRNA. For each duplex, the two complementary oligonucleotides encoding these sequences (see *Reagent Table*) were annealed as follows: Each

oligonucleotide was resuspended to a final 50 µM concentration. Then, 10 µl of each oligonucleotide in the doublex was mixed, to 20 µl total. Annealing was done in the thermocycler, at 95°C for 5 min, 55°C for 15 min, 25°C for 15 min. The annealed oligonucleotides were inserted into the gRNA entry vector (plasmid YTK050) of the MoClo-YTK plasmid kit (Lee *et al.*, 2015), through the "Golden Gate" cloning strategies described in (Akhmetov *et al.*, 2018), for 42°C for 5 min, 60°C for 5 min. The resulting plasmids (FAS1_cRNA-1_ENTRY, FAS1_cRNA-2_ENTRY, FAS1_cRNA-3_ENTRY, respectively) were sequenced with primer t0-ter_FWD (see *Reagent Table*) to verify the cloning of the gRNA sequences.

Cassette plasmid assembly. The dCas13d-dsRBD-APEX2_001 plasmid was mixed in a single-pot "Golden Gate" assembly with T7 ligase and *Bsa*I, and with plasmids YTK002 (conLS; connector), YTK067 (conR1; connector), YTK009 (*pTDH3*; promoter), YTK063 (*tADH1*; terminator), YTK074 (*URA3*; yeast selection marker), YTK081 (*CEN6/ARS4*; yeast maintenance), YTK083 (AmpR-ColE1; bacterial selection and maintenance), all of which are in the MoClo-YTK plasmid kit (Lee *et al.*, 2015), which was a gift from John Dueber (Addgene kit # 1000000061). The assembly reaction conditions were 50 cycles: 37°C for 2 min, 16°C for 5 min followed by 60°C for 5 min, and 80°C for 10 min.

The assembled plasmid (APEX_TU1) encoded a transcriptional unit for dCas13d-dsRBD-APEX2 expression in yeast, from a stably maintained (*CEN6/ARS4*) plasmid. We transformed yeast cells (BY4742 strain) with the APEX_TU1 plasmid. The ends of the insert in the plasmid were sequenced with primers AmpR-FWD and pBR322ori-FWD (see *Reagent Table*). Then, we verified that the transformants express a protein recognized by an anti-V5 antibody conjugated with HRP (Invitrogen catalogue# R96125; see *Reagent Table*; used at a 1:5000 dilution) with an apparent molecular mass of around 153,650.71 Da, expected for the dCas13d-dsRBD-APEX2 protein (unpublished data).

The *FAS1* gRNA cassettes were assembled individually, as described above for APEX_TU1, with T7 ligase and *Bsa*I. Each reaction contained the FAS1_cRNA entry plasmid of interest and plasmids YTK003 (conL1; connector), YTK072 (conRE; connector), YTK083 (AmpR-ColE1; bacterial selection and maintenance), from the MoClo-YTK plasmid kit, yielding plasmids FAS1-1_TU2, and FAS1-2_TU2, respectively. The correct inserts were validated by sequencing, with primers AmpR-FWD and pBR322ori-FWD (see *Reagent Table*).

To generate FAS1-3_TU2, we first PCR-amplified the corresponding insert using FAS1-3_ENTRY as a template, and primers 050_L1 and 050_RE (see *Reagent Table*; which encode the appropriate *Bsm*BI sites for the next bicistronic assembly).

Bicistronic plasmid assembly and yeast expression. To drive expression of dCas13d-dsRBD-APEX2 and each of the *FAS1* cRNAs off the same plasmid in yeast, we combined T7 ligase and *Bsm*BI plasmids APEX_TU1, YTK096, and one of FAS1-1_TU2 plasmid, FAS1-2_TU2 plasmid, or the FAS1-3_TU2 PCR fragment. These assembly reaction conditions were 50 cycles: 42°C for 2 min, 16°C for 5 min followed by 60°C for 5 min and 80°C for 10 min. They yielded plasmids APEX-FAS1-1_INT, APEX-FAS1-2_INT, APEX-FAS1-3_INT; respectively. Correct assembly was validated by sequencing, with primers FOR_6 and 050_RE (see *Reagent Table*). Plasmids APEX-FAS1-1_INT, APEX-FAS1-2_INT, and APEX-FAS1-3_INT were each digested with *Not*I and used to transform strain BY4742, yielding strains SCMSP244, SCMSP245, and SCMSP246, respectively. Each of these strains carries an integration of the bicistronic assembly into the *URA3* locus. The strains were validated by APEX protein expression, through immunoblotting against the V5 epitope, and sequencing of the chromosomal locus for the presence of the correct gRNA. Lastly, we also ensured that the APEX fusion was active in these strains, using the Amplex Red assay described previously (Turnšek *et al.*, 2021), generating the strongly fluorescent resorufin (Dębski *et al.*, 2016), as shown in Figure 1.

Yeast mutants. Single gene haploid deletion strains, lacking *ARC1*, *SRO9*, *SSD1*, or *TDH3*, were commercially available (see *Reagent Table*). Their genotype was validated by PCR, to confirm that the gene of interest was absent and replaced by the appropriate marker. These strains were crossed with a commercially available *FAS1-TAP* strain (see *Reagent Table*), sporulated, and dissected to obtain the corresponding haploid deletion mutant of the mRNA-binding protein carrying a *FAS1-TAP* allele.

Centrifugal elutriation and cell size measurements

All methods have been described previously (Hoose *et al.*, 2012; Soma *et al.*, 2014; Blank *et al.*, 2017b, 2020; Maitra *et al.*, 2020). Briefly, to collect enough cells for the LC–MS/MS measurements after proximity labeling, elutriated G1 cells were allowed to progress in the cell cycle until they reached the desired cell size. At that point, they were quenched (with 100 µg/ml cycloheximide) and frozen away, and later pooled with cells of similar size. Overall, we had to collect 54 individual samples, to generate the 18 pools shown in Figure 3B.

For other elutriation experiments (e.g., see Figures 4 and 5; Supplemental Figure S1), only an early G1 elutriated fraction was collected, from which samples were taken at regular intervals as the cells progressed in the cell cycle.

Proximity labeling reactions

For each labeling reaction, 1E+09 cells collected, stored at –80°C in freezing buffer (15% glycerol, 150 mM potassium acetate, 2 mM magnesium acetate, 20 mM HEPES/sodium hydroxide pH 7.2, 0.5% [wt/vol] glucose, 100 µg/ml cycloheximide), and were thawed on ice. The cells were washed in 10 ml 0.1 M MES/sodium hydroxide pH 6.5, 100 µg/ml cycloheximide, resuspended in 2 ml of this buffer containing 0.01% digitonin (10 µl added from a 20 mg/ml digitonin stock in Dimethylsulfoxide [DMSO]), and incubated in a 30°C shaking water bath for 30 min (Cordeiro and Freire, 1995). The cells were then collected by a brief centrifugation, washed with 10 ml of ice-cold 1.2 M sorbitol/ phosphate-buffered saline (PBS) solution, resuspended in 2 ml of 1.2 M sorbitol/PBS containing 2.5 mM phenol-biotin (10 µl added from a 0.5M stock in DMSO, stored at –80°C), 20 µl from a 20 U/µl stock of SUPERase RNase Inhibitor, 20 µl from a 10 mg/ml stock of cycloheximide, and protease inhibitors, and incubated on ice for 90 min (Turnšek *et al*, 2021). About 15 min before the end of the 90-min incubation on ice, a quenching solution was prepared by mixing the following: 200 µl Trolox (from a 0.5 M stock in DMSO, stored at –80°C); 200 µl sodium azide (from a 1 M stock in water, stored at –80°C); 2 ml of a 10 mM sodium ascorbate solution in PBS, prepared fresh. Also before the end of the 90-min incubation on ice, a 0.2 M stock of hydrogen peroxide was prepared (by dilution of a 30% [9.8 M] hydrogen peroxide solution; stored at 4°C). At the end of the 90-min incubation on ice, the cells were exposed to 2 mM hydrogen peroxide (20 µl were added to the 2 ml cell suspension from the 0.2 M solution), vortexed briefly, and incubated on ice for 2 min. The reaction was stopped by adding 2 ml of the freshly prepared quenching solution described above. The cells were collected by centrifugation, washed with 10 ml of Tris-buffered saline (TBS), pH 7.5, and resuspended in 3 ml of TBS, pH 7.5. Then 1.5 ml of glass beads was added to each tube, to break the cells with six

cycles of 30-s vortexing–30 s on ice. The cells were centrifuged for 10 min in the cold, and the supernatants transferred to 15 ml screw-cap tubes.

To isolate the biotinylated proteins for mass spectrometry, 0.2 ml of beads (Dynabeads MyOne Streptavidin C1; Thermo Fisher Scientific, catalogue #: 65001) were added to each tube, and incubated on a rotisserie mixer for 1 h at room temperature. A magnetic rack was used to isolate the beads and remove the supernatant. The beads were washed twice with 10 ml TBS, 2 M urea, pH 7.5, once with 10 ml 0.1 M ammonium carbonate pH 7.7, and resuspended in 0.5 ml 0.1 M ammonium carbonate pH 7.7.

The APEX labeling reactions shown in Figure 2 were done as described above but from 1E+08 cells, with all the reaction volumes reduced 10-fold, and then processed for immunoblotting as described below. Because the APEX-catalyzed reaction is H_2O_2-dependent, we tested varied times of the reaction. We concluded that a 2-min reaction yielded optimal labeling in the shortest time tested (Figure 2).

LC–MS/MS

The beads were washed three times with 200 µl of 25 mM ammonium bicarbonate. After the final wash, 200 µl of 25 mM ammonium bicarbonate was added along with 2 µg of proteomics-grade trypsin (2 µl of a 1 µg/µl solution) and incubated for a day at 37°C with intermittent vortexing. An aliquot of the supernatants from the resultant samples were diluted two-fold in Solvent A (95/5% water/acetonitrile containing 0.1% formic acid); and 1 µl injected for analysis by LC–MS/MS. The nanoLC–MS consisted of an UltiMate 3000 Nano LC System and an LTQ-Orbitrap Elite mass spectrometer (Thermo Fisher Scientific, San Jose, CA). Reversed-phase liquid chromatography was performed using a homemade 33 cm × 75 µm ID column packed with XBridgeTM BEH C18 media (2.5 µm, 130 Å). The flow rate was maintained at 200 nL/min. Solvent A and B (95/5% acetonitrile/water containing 0.1% formic acid) were used to establish the 160-min gradient elution timetable: isocratic at 5% B for 30 min, 5–55% B over 70 min, followed by 55–99% B in 5 min where it was maintained for 10 min, and finally returned to 5% B over 5 min for a 40 min reequilibration time. The LTQ-Orbitrap Elite mass spectrometer instrument was operated in positive mode with a 2.6 kv applied spray voltage. The temperature of the ion transfer capillary was 300°C. One microscan was set for each MS and MS/MS scan. A full scan MS acquired in the range $300 \leq m/z \leq 2000$ was followed by 10 data-dependent MS/MS events on the 10 most intense ions. The mass resolution was set at 60,000 for full MS. The dynamic exclusion function was set as follows: repeat count, 1; repeat duration, 30 s; exclusion duration, 30 s. HCD was performed using normalized collision energy of 35% and the activation time was set as 0.1 ms. Mascot software (Matrix Science, Boston, MA) was used for protein identification and quantitation. The mass spectrometry proteomics data have been deposited to the ProteomeXchange Consortium via the PRIDE (Perez-Riverol *et al.*, 2022) partner repository with the dataset identifier PXD041908. To identify proteins that were preferentially associated with the *FAS1* mRNA in the G1 phase or in the G2 phase, each strain was analyzed separately with the robust bootstrap ANOVA. The input values used in each case are shown in Supplemental File S1/Sheets 6, 7, and 8. The output values and the fold change are in Supplemental File S1/Sheet 3, and plotted in the volcano plots shown in Figure 3C.

Immunoprecipitations and pull downs

dCas13d-dsRBD-APEX2-V5. Exponentially proliferating cells were quenched with 100 µg/ml cycloheximide. They were then collected by centrifugation and washed with freezing buffer (15% glycerol, 150 mM potassium acetate, 2 mM magnesium acetate, 20 mM HEPES/sodium hydroxide pH 7.2, 0.5% ($^{wt/vol}$) glucose, 100 µg/ml cycloheximide), resuspended in the same freezing buffer (1E+08 cells in 60 µl buffer), and stored at −80°C until further use (Singer-Krüger *et al.*, 2020). The cells were washed in 1 ml of RIP buffer (150 mM Potassium chloride, 25 mM Tris pH 7.4, 5 mM ethylenediaminetetraacetic acid, 0.5 mM dithiothreitol, 0.5% IGEPAL CA-630), and resuspended in 0.6 ml of RIP buffer containing 100 U/mL RNAse inhibitor SUPERase•in (Thermo Fisher Scientific; catalogue #: AM2694, see *Reagent Table*) and protease inhibitor cocktail (Millipore Sigma; catalogue #: 11836170001; the RNAse and protease inhibitors were added fresh). About 0.250 ml of glass beads was added and vortexed at the maximum speed for 30 s, then placed on ice for 30 s. The vortex–ice cycle was repeated for a total of six times to break the cells. The supernatant was collected after a centrifugation at 5000 rpm for 5 min, and clarified with another centrifugation at 12,000 rpm for 2 min. The clarified supernatant was removed and 0.15 ml was stored at −80°C, to serve as "input" control. To the rest, 10 µl of agarose-α-V5 beads were added, and incubated at 4°C on a tube rotator for 1–2 h. The beads were pelleted at 1000 rpm for 1 min, and the supernatant was removed. The beads were washed with 0.5 ml RIP buffer, and pelleted as before. Two additional such washes were performed, and the beads were resuspended in 130 µl of RIP buffer and stored at −80°C, before RNA isolation and ddPCR.

TAP-tagged proteins. Because many RNA-binding proteins are found in stress granules, we adapted an approach described previously to generate cell extracts that recover such structures (Jain *et al.*, 2016). Briefly, for each TAP-tagged strain, cells from 1 L of culture (in YPD) was harvested and resuspended in 10 ml of lysis buffer (10 mM Tris-HCl pH 7.5, 100 mM sodium chloride, 1.5 mM magnesium chloride, 0.5% NP-40), with 1:5000 antifoam emulsion and protease inhibitor cocktail added. 5 ml of glass beads was added and the cells were lysed by three cycles of vortexing for 2 min followed by 2 min on ice. The lysates were centrifuged at 850 × *g* for 2 min and the supernatants collected. Then 0.2 ml of washed IgG Sepharose six Fast Flow beads (Millipore Sigma, catalogue #: GE17-0969-01) were added to each sample and incubated on a rotisserie mixer for 0.5 h at room temperature. The beads were washed three times with a buffer containing 10 mM Tris-HCl pH 7.5, 100 mM sodium chloride, 1.5 mM magnesium chloride, 0.1% NP-40. The beads were resuspended in 500 µl of the same buffer and stored at −80°C, before RNA isolation and ddPCR.

Immunoblotting

For the samples shown in Figure 2, the cells were collected by centrifugation, resuspended in 0.1 ml 0.1 N sodium hydroxide, and incubated at room temperature for 5 min. An equal volume of 2× Laemmli buffer (65.8 mM Tris-HCl, pH 6.8, 2.1% sodium dodecyl sulfate, 26.3% $^{wt/vol}$ glycerol, 0.01% bromophenol blue) was added to the samples before SDS–PAGE. Biotinylated proteins were detected with a streptavidin–HRP conjugate (Millipore-Sigma, catalogue #: OR03L-200UG), used at 1:2000 dilution (see *Reagent Table*).

To detect TAP-tagged proteins (see Figure 4; Supplemental Figure S1), protein extracts were made as described previously (Amberg *et al.*, 2006), and resolved on Tris-Glycine SDS–PAGE gels. To detect the tagged proteins with the peroxidase anti-peroxidase (PAP) reagent (Millipore-Sigma; catalogue #: P1291, used at 1:5000 dilution), we used immunoblots from extracts of the indicated

strains, as we described previously (Blank *et al.*, 2017b, 2020; Maitra *et al.*, 2020, 2022). Loading was measured with an anti-Pgk1p primary antibody (Thermo Fisher Scientific; catalogue #: 459250) used at 1:5000 dilution, and a secondary antimouse HRP-conjugated antibody (Abcam; catalogue #: ab205719) used at 1:5000 dilution. Imaging and quantification was done as described previously (Blank *et al.*, 2017b, 2020; Maitra *et al.*, 2020, 2022).

Digital droplet PCR

All methods have been described previously (Maitra *et al*, 2022). Briefly, the ddPCR reaction mixture was prepared using the Taqman hydrolysis probes labeled with FAM (for *FAS1*) and VIC (for *UBC6*) reporter fluorophores. Transcript levels of *FAS1* were normalized against the corresponding transcript levels of *UBC6*.

Statistical analysis, sample size, and replicates

For sample-size estimation, no explicit power analysis was used. There was also no randomization or blinding during sample analysis. All the replicates in every experiment shown were biological ones, from independent cultures. A minimum of three biological replicates were analyzed in each case, as indicated in each corresponding figure legends. The robust bootstrap ANOVA was used to compare different populations via the t1waybt function, and the posthoc tests via the mcppb20 function, of the WRS2 R language package (Wilcox, 2011; Mair and Wilcox, 2020). Note that with the robust bootstrap ANOVA exact p values < 0.0001 were not calculated. We also used nonparametric statistical methods, as indicated in each case. The Kruskal-Wallis and posthoc Nemenyi tests were done with the posthoc.kruskal.nemenyi.test function of the PMCMR R language package. No data or outliers were excluded from any analysis.

Data availability

Strains and plasmids are available upon request. The authors affirm that all data necessary for confirming the conclusions of the article are present within the article, figures, and tables. LC–MS/MS data are available via ProteomeXchange with identifier PXD041908.

ACKNOWLEDGMENTS

This research was supported by a grant from the NIH (GM123139) to M.P. LC–MS/MS analyses were carried out at the UTSA Mass Spectrometry & Proteomics Core.

REFERENCES

Abudayyeh OO, Gootenberg JS, Essletzbichler P, Han S, Joung J, Belanto JJ, Verdine V, Cox DBT, Kellner MJ, Regev A, *et al.* (2017). RNA targeting with CRISPR-Cas13. Nature 550, 280–284.

Akhmetov A, Laurent JM, Gollihar J, Gardner EC, Garge RK, Ellington AD, Kachroo AH, Marcotte EM (2018). Single-step precision genome editing in yeast using CRISPR-Cas9. Bio-Protoc 8, e2765.

Albuquerque CP, Smolka MB, Payne SH, Bafna V, Eng J, Zhou H (2008). A multidimensional chromatography technology for in-depth phosphoproteome analysis. Mol Cell Proteomics 7, 1389–1396.

Al-Feel W, Chirala SS, Wakil SJ (1992). Cloning of the yeast FAS3 gene and primary structure of yeast acetyl-CoA carboxylase. Proc Natl Acad Sci USA 89, 4534–4538.

Amberg DC, Burke DJ, Strathern JN (2006). Yeast protein extracts. CSH Protoc, https://doi.org/10.1101/pdb.prot4152.

Aramayo R, Polymenis M (2017). Ribosome profiling the cell cycle: lessons and challenges. Curr Genet 63, 959–964.

Back S, Gorman AW, Vogel C, Silva GM (2019). Site-specific K63 ubiquitinomics provides insights into translation regulation under stress. J Proteome Res 18, 309–318.

Bayne RA, Jayachandran U, Kasprowicz A, Bresson S, Tollervey D, Wallace EWJ, Cook AG (2022). Yeast Ssd1 is a non-enzymatic member of the RNase II family with an alternative RNA recognition site. Nucleic Acids Res 50, 2923–2937.

Beckmann BM, Horos R, Fischer B, Castello A, Eichelbaum K, Alleaume A-M, Schwarzl T, Curk T, Foehr S, Huber W, *et al.* (2015). The RNA-binding proteomes from yeast to man harbour conserved enigmRBPs. Nat Commun 6, 10127.

Bhagwat NR, Owens SN, Ito M, Boinapalli JV, Poa P, Ditzel A, Kopparapu S, Mahalawat M, Davies OR, Collins SR, *et al.* (2021). SUMO is a pervasive regulator of meiosis. eLife 10, e57720.

Blank HM, Maitra N, Polymenis M (2017a). Lipid biosynthesis: When the cell cycle meets protein synthesis? Cell Cycle 16, 905–906.

Blank HM, Perez R, He C, Maitra N, Metz R, Hill J, Lin Y, Johnson CD, Bankaitis VA, Kennedy BK, *et al.* (2017b). Translational control of lipogenic enzymes in the cell cycle of synchronous, growing yeast cells. EMBO J 36, 487–502.

Blank HM, Papoulas O, Maitra N, Garge R, Kennedy BK, Schilling B, Marcotte EM, Polymenis M (2020). Abundances of transcripts, proteins, and metabolites in the cell cycle of budding yeast reveal coordinate control of lipid metabolism. Mol Biol Cell 31, 1069–1084.

Bonafé N, Gilmore-Hebert M, Folk NL, Azodi M, Zhou Y, Chambers SK (2005). Glyceraldehyde-3-phosphate dehydrogenase binds to the AU-Rich 3′ untranslated region of colony-stimulating factor-1 (CSF-1) messenger RNA in human ovarian cancer cells: possible role in CSF-1 posttranscriptional regulation and tumor phenotype. Cancer Res 65, 3762–3771.

Cai Y, Futcher B (2013). Effects of the yeast RNA-binding protein Whi3 on the half-life and abundance of CLN3 mRNA and other targets. PLoS One 8, e84630.

Cao L, Yu L, Guo Z, Shen A, Guo Y, Liang X (2014). N-Glycosylation site analysis of proteins from Saccharomyces cerevisiae by using hydrophilic interaction liquid chromatography-based enrichment, parallel deglycosylation, and mass spectrometry. J Proteome Res 13, 1485–1493.

Castello A, Hentze MW, Preiss T (2015). Metabolic enzymes enjoying new partnerships as RNA-binding proteins. Trends Endocrinol Metab 26, 746–757.

Castello A, Fischer B, Frese CK, Horos R, Alleaume A-M, Foehr S, Curk T, Krijgsveld J, Hentze MW. (2016). Comprehensive identification of RNA-binding domains in human cells. Mol Cell 63, 696–710.

Clemm von Hohenberg K, Müller S, Schleich S, Meister M, Bohlen J, Hofmann TG, Teleman AA (2022). Cyclin B/CDK1 and Cyclin A/CDK2 phosphorylate DENR to promote mitotic protein translation and faithful cell division. Nat Commun 13, 668.

Cordeiro C, Freire AP (1995). Digitonin permeabilization of Saccharomyces cerevisiae cells for in situ enzyme assay. Anal Biochem 229, 145–148.

Dębski D, Smulik R, Zielonka J, Michałowski B, Jakubowska M, Dębowska K, Adamus J, Marcinek A, Kalyanaraman B, Sikora A (2016). Mechanism of oxidative conversion of Amplex® Red to resorufin: pulse radiolysis and enzymatic studies. Free Radic Biol Med 95, 323–332.

Di Talia S, Skotheim JM, Bean JM, Siggia ED, Cross FR (2007). The effects of molecular noise and size control on variability in the budding yeast cell cycle. Nature 448, 947–951.

Dollenmaier G, Weitz M (2003). Interaction of glyceraldehyde-3-phosphate dehydrogenase with secondary and tertiary RNA structural elements of the hepatitis A virus 3′ translated and non-translated regions. J Gen Virol 84, 403–414.

Elliott SG, McLaughlin CS (1978). Rate of macromolecular synthesis through the cell cycle of the yeast Saccharomyces cerevisiae. Proc Natl Acad Sci USA 75, 4384–4388.

Elliott SG, Warner JR, McLaughlin CS (1979). Synthesis of ribosomal proteins during the cell cycle of the yeast Saccharomyces cerevisiae. J Bacteriol 137, 1048–1050.

Engler C, Kandzia R, Marillonnet S (2008). A one pot, one step, precision cloning method with high throughput capability. PLoS ONE 3, e3647.

Engler C, Gruetzner R, Kandzia R, Marillonnet S (2009). Golden gate shuffling: a one-pot DNA shuffling method based on type IIs restriction enzymes. PloS One 4, e5553.

Frankovsky J, Keresztesová B, Bellová J, Kunová N, Čanigová N, Hanakova K, Bauer JA, Ondrovičová G, Lukáčová V, Sivákova B, *et al.* (2021). The yeast mitochondrial succinylome: Implications for regulation of mitochondrial nucleoids. J Biol Chem 297, 101155.

Han S, Zhao BS, Myers SA, Carr SA, He C, Ting AY (2020). RNA-protein interaction mapping via MS2- or Cas13-based APEX targeting. Proc Natl Acad Sci USA 117, 22068–22079.

Henriksen P, Wagner SA, Weinert BT, Sharma S, Bacinskaja G, Rehman M, Juffer AH, Walther TC, Lisby M, Choudhary C (2012).

Proteome-wide analysis of lysine acetylation suggests its broad regulatory scope in Saccharomyces cerevisiae. Mol Cell Proteomics MCP 11, 1510–1522.
Hentze MW, Castello A, Schwarzl T, Preiss T (2018). A brave new world of RNA-binding proteins. Nat Rev Mol Cell Biol 19, 327–341.
Hentze MW, Preiss T (2010). The REM phase of gene regulation. Trends Biochem Sci 35, 423–426.
Hogan DJ, Riordan DP, Gerber AP, Herschlag D, Brown PO (2008). Diverse RNA-binding proteins interact with functionally related sets of RNAs, suggesting an extensive regulatory system. PLoS Biol 6, e255.
Holt LJ, Tuch BB, Villén J, Johnson AD, Gygi SP, Morgan DO (2009). Global analysis of Cdk1 substrate phosphorylation sites provides insights into evolution. Science 325, 1682–1686.
Hoose SA, Rawlings JA, Kelly MM, Leitch MC, Ababneh QO, Robles JP, Taylor D, Hoover EM, Hailu B, McEnery KA, *et al*. (2012). A systematic analysis of cell cycle regulators in yeast reveals that most factors act independently of cell size to control initiation of division. PLoS Genet 8, e1002590.
Hwang J, Espenshade PJ (2016). Proximity-dependent biotin labelling in yeast using the engineered ascorbate peroxidase APEX2. Biochem J 473, 2463–2469.
Ishihama Y, Oda Y, Tabata T, Sato T, Nagasu T, Rappsilber J, Mann M (2005). Exponentially modified protein abundance index (emPAI) for estimation of absolute protein amount in proteomics by the number of sequenced peptides per protein. Mol Cell Proteomics MCP 4, 1265–1272.
Jain S, Wheeler JR, Walters RW, Agrawal A, Barsic A, Parker R (2016). ATPase-Modulated stress granules contain a diverse proteome and substructure. Cell 164, 487–498.
Kaeberlein M, Guarente L (2002). Saccharomyces cerevisiae MPT5 and SSD1 function in parallel pathways to promote cell wall integrity. Genetics 160, 83–95.
Kaiser C, Michaelis S, Mitchell A (1994). Methods in yeast genetics : A Cold Spring Harbor Laboratory course manual 1994th ed. Cold Spring Harbor, NY: Cold Spring Harbor Laboratory Press, 207.
Lanz MC, Yugandhar K, Gupta S, Sanford EJ, Faça VM, Vega S, Joiner AMN, Fromme JC, Yu H, Smolka MB (2021). In-depth and 3-dimensional exploration of the budding yeast phosphoproteome. EMBO Rep 22, e51121.
Lee ME, DeLoache WC, Cervantes B, Dueber JE (2015). A highly characterized yeast toolkit for modular, multipart assembly. ACS Synth Biol 4, 975–986.
Li Y, Liu K, Zhou Y, Yang J, Zou P (2020). Protocol for proximity-dependent proteomic profiling in yeast cells by APEX and Alk-Ph probe. STAR Protoc 1, 100137.
Li Y, Liu S, Cao L, Luo Y, Du H, Li S, Zhang Z, Guo X, Tian W, Wong CC, *et al*. (2021). CBRPP: a new RNA-centric method to study RNA-protein interactions. RNA Biol 18, 1608–1621.
MacGilvray ME, Shishkova E, Place M, Wagner ER, Coon JJ, Gasch AP (2020). Phosphoproteome response to dithiothreitol reveals unique versus shared features of Saccharomyces cerevisiae stress responses. J Proteome Res 19, 3405–3417.
Mair P, Wilcox R (2020). Robust statistical methods in R using the WRS2 package. Behav Res Methods 52, 464–488.
Maitra N, He C, Blank HM, Tsuchiya M, Schilling B, Kaeberlein M, Aramayo R, Kennedy BK, Polymenis M (2020). Translational control of one-carbon metabolism underpins ribosomal protein phenotypes in cell division and longevity. eLife 9, e53127.
Maitra N, Hammer S, Kjerfve C, Bankaitis VA, Polymenis M (2022). Translational control of lipogenesis links protein synthesis and phosphoinositide signaling with nuclear division in Saccharomyces cerevisiae. Genetics 220, iyab171.
Matia-González AM, Laing EE, Gerber AP (2015). Conserved mRNA-binding proteomes in eukaryotic organisms. Nat Struct Mol Biol 22, 1027–1033.
McAlister L, Holland MJ (1985). Isolation and characterization of yeast strains carrying mutations in the glyceraldehyde-3-phosphate dehydrogenase genes. J Biol Chem 260, 15013–15018.
Mills EW, Green R (2017). Ribosomopathies: There's strength in numbers. Science 358, eaan2755.
Mitchell SF, Jain S, She M, Parker R (2013). Global analysis of yeast mRNPs. Nat Struct Mol Biol 20, 127–133.
Perez-Riverol Y, Bai J, Bandla C, García-Seisdedos D, Hewapathirana S, Kamatchinathan S, Kundu DJ, Prakash A, Frericks-Zipper A, Eisenacher M, *et al*. (2022). The PRIDE database resources in 2022: a hub for mass spectrometry-based proteomics evidences. Nucleic Acids Res 50, D543–D552.
Polymenis M (2022a). mRNA-binding proteins and cell cycle progression. Trends Genet TIG 38, 797–800.
Polymenis M (2022b). Two from one: A short introduction to cell division mechanisms, Hoboken, NJ: John Wiley & Sons, 53–56.
Rødkær SV, Pultz D, Brusch M, Bennetzen MV, Falkenby LG, Andersen JS, Færgeman NJ (2014). Quantitative proteomics identifies unanticipated regulators of nitrogen- and glucose starvation. Mol Biosyst 10, 2176–2188.
Rodríguez-Pascual F, Redondo-Horcajo M, Magán-Marchal N, Lagares D, Martínez-Ruiz A, Kleinert H, Lamas S (2008). Glyceraldehyde-3-phosphate dehydrogenase regulates endothelin-1 expression by a novel, redox-sensitive mechanism involving mRNA stability. Mol Cell Biol 28, 7139–7155.
Ryazanov AG (1985). Glyceraldehyde-3-phosphate dehydrogenase is one of the three major RNA-binding proteins of rabbit reticulocytes. FEBS Lett 192, 131–134.
Santos A, Wernersson R, Jensen LJ (2015). Cyclebase 3.0: a multi-organism database on cell-cycle regulation and phenotypes. Nucleic Acids Res 43, D1140–4.
Schneiter R, Guerra CE, Lampl M, Gogg G, Kohlwein SD, Klein HL (1999). The Saccharomyces cerevisiae hyperrecombination mutant hpr1Delta is synthetically lethal with two conditional alleles of the acetyl coenzyme A carboxylase gene and causes a defect in nuclear export of polyadenylated RNA. Mol Cell Biol 19, 3415–3422.
Schrader JM, Li G-W, Childers WS, Perez AM, Weissman JS, Shapiro L, McAdams HH (2016). Dynamic translation regulation in Caulobacter cell cycle control. Proc Natl Acad Sci USA 113, E6859–E6867.
Sellami M, Prévost G, Bonnet J, Dirheimer G, Gangloff J (1985). Isolation and characterization of the yeast aspartyl-tRNA synthetase gene. Gene 40, 349–352.
Simos G, Segref A, Fasiolo F, Hellmuth K, Shevchenko A, Mann M, Hurt EC (1996). The yeast protein Arc1p binds to tRNA and functions as a cofactor for the methionyl- and glutamyl-tRNA synthetases. EMBO J 15, 5437–5448.
Singer-Krüger B, Fröhlich T, Franz-Wachtel M, Nalpas N, Macek B, Jansen R-P (2020). APEX2-mediated proximity labeling resolves protein networks in Saccharomyces cerevisiae cells. FEBS J 287, 325–344.
Singh R, Green MR (1993). Sequence-specific binding of transfer RNA by glyceraldehyde-3-phosphate dehydrogenase. Science 259, 365–368.
Sobel SG, Wolin SL (1999). Two yeast La motif-containing proteins are RNA-binding proteins that associate with polyribosomes. Mol Biol Cell 10, 3849–3862.
Soma S, Yang K, Morales MI, Polymenis M (2014). Multiple metabolic requirements for size homeostasis and initiation of division in *Saccharomyces cerevisiae*. Microb Cell 1, 256–266.
Soulard A, Cremonesi A, Moes S, Schütz F, Jenö P, Hall MN (2010). The rapamycin-sensitive phosphoproteome reveals that TOR controls protein kinase A toward some but not all substrates. Mol Biol Cell 21, 3475–3486.
Spellman PT, Sherlock G, Zhang MQ, Iyer VR, Anders K, Eisen MB, Brown PO, Botstein D, Futcher B (1998). Comprehensive identification of cell cycle-regulated genes of the yeast Saccharomyces cerevisiae by microarray hybridization. Mol Biol Cell 9, 3273–3297.
Stonyte V, Boye E, Grallert B (2018). Regulation of global translation during the cell cycle. J Cell Sci 131, jcs220327.
Stumpf CR, Moreno MV, Olshen AB, Taylor BS, Ruggero D (2013). The translational landscape of the mammalian cell cycle. Mol Cell 52, 574–582.
Swaney DL, Beltrao P, Starita L, Guo A, Rush J, Fields S, Krogan NJ, Villén J (2013). Global analysis of phosphorylation and ubiquitylation cross-talk in protein degradation. Nat Methods 10, 676–682.
Takhaveev V, Özsezen S, Smith EN, Zylstra A, Chaillet ML, Chen H, Papagiannakis A, Milias-Argeitis A, Heinemann M (2023). Temporal segregation of biosynthetic processes is responsible for metabolic oscillations during the budding yeast cell cycle. Nat Metab 5, 294–313.
Tanenbaum ME, Stern-Ginossar N, Weissman JS, Vale RD (2015). Regulation of mRNA translation during mitosis. Elife 4, e07957.
Turnšek J, Brunson JK, Viedma M, Deerinck TJ, Horák A, Oborník M, Bielinski VA, Allen AE (2021). Proximity proteomics in a marine diatom reveals a putative cell surface-to-chloroplast iron trafficking pathway. eLife 10, e52770.
Wang K, Zhou YJ, Liu H, Cheng K, Mao J, Wang F, Liu W, Ye M, Zhao ZK, Zou H (2015). Proteomic analysis of protein methylation in the yeast Saccharomyces cerevisiae. J Proteomics 114, 226–233.

Weinert BT, Schölz C, Wagner SA, Iesmantavicius V, Su D, Daniel JA, Choudhary C (2013). Lysine succinylation is a frequently occurring modification in prokaryotes and eukaryotes and extensively overlaps with acetylation. Cell Rep 4, 842–851.
Wessels H-H, Méndez-Mancilla A, Guo X, Legut M, Daniloski Z, Sanjana NE (2020). Massively parallel Cas13 screens reveal principles for guide RNA design. Nat Biotechnol 38, 722–727.
Wilcox RR (2011). Introduction to robust estimation and hypothesis testing. Amsterdam, Netherlands: Academic Press.
Zhang C, Konermann S, Brideau NJ, Lotfy P, Wu X, Novick SJ, Strutzenberg T, Griffin PR, Hsu PD, Lyumkis D (2018). Structural basis for the RNA-guided ribonuclease activity of CRISPR-Cas13d. Cell 175, 212–223.e17.
Zhou X, Li W, Liu Y, Amon A (2021). Cross-compartment signal propagation in the mitotic exit network. eLife 10, e63645.
Zielinska DF, Gnad F, Schropp K, Wiśniewski JR, Mann M (2012). Mapping N-glycosylation sites across seven evolutionarily distant species reveals a divergent substrate proteome despite a common core machinery. Mol Cell 46, 542–548.